



Adaptive mesh refinement method-based large eddy simulation for the flow over circular cylinder at $Re_D = 3900$

Jinlan Gou, Xinrong Su & Xin Yuan

To cite this article: Jinlan Gou, Xinrong Su & Xin Yuan (2018) Adaptive mesh refinement method-based large eddy simulation for the flow over circular cylinder at $Re_D = 3900$, International Journal of Computational Fluid Dynamics, 32:1, 1-18, DOI: [10.1080/10618562.2018.1461845](https://doi.org/10.1080/10618562.2018.1461845)

To link to this article: <https://doi.org/10.1080/10618562.2018.1461845>



Published online: 20 Apr 2018.



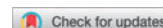
Submit your article to this journal [↗](#)



Article views: 123



View Crossmark data [↗](#)



Adaptive mesh refinement method-based large eddy simulation for the flow over circular cylinder at $Re_D = 3900$

Jinlan Gou^{a,b}, Xinrong Su^a and Xin Yuan^a

^aKey Laboratory for Thermal Science and Power Engineering of Ministry of Education, Tsinghua University, Beijing, P. R. China; ^bWuhan 2nd Ship Design and Research Institute, Wuhan, P. R. China

ABSTRACT

With the development of computational power, large eddy simulation (LES) method is increasingly used in simulating complex flow. However, there still exist many factors affecting the LES quality and appropriate mesh resolution is among one of them. This work aims to develop an automatic procedure to refine the LES mesh by combining adaptive mesh refinement (AMR) and LES quality criteria. An LES refinement criterion is developed by estimating the proper grid length scale which meets the accuracy requirement of LES method. With this criterion, the baseline mesh is automatically refined with the AMR method. In this work, an efficient one-shot refinement strategy is also proposed to reduce the overall simulation time. Current AMR-based LES method is verified with the typical LES test case about the flow past circular cylinder at $Re_D = 3900$. Results show that the automatically refined mesh provides systematically better agreement with experimental results and with current method the balance between accuracy and computational expense for LES can be obtained.

ARTICLE HISTORY

Received 23 June 2017
Accepted 29 March 2018

KEYWORDS

LES; AMR; filter width; modelled turbulent kinetic energy ratio; circular cylinder

1. Introduction

Comparing to the traditional Reynolds-averaged Navier-Stokes equations (RANS) method, large eddy simulation (LES) and hybrid RANS/LES are promising methods to improve the prediction accuracy with affordable computing resources and recently they are increasingly employed in both academic and industrial applications, see Raverdy et al. (2003), Michelassi, Wissink, and Rodi (2003), Sarkar and Voke (2006), You et al. (2006), Ray and Dawes (2009), Léonard, Gicquel, and Gourdain (2010), McMullan and Page (2011), Taghavi-Zenouz and Eslami (2012), McMullan and Page (2012), Lardeau, Leschziner, and Zaki (2012), Duchaine et al. (2013), Riéra et al. (2013), Memory, Chen, and Bons (2016), Papadogiannis et al. (2016), Wang et al. (2017), Lin, Su, and Yuan (2018) for examples. Despite the development for several decades, LES and hybrid RANS/LES still have some unresolved problems in simulating the flow in complex geometry. Many factors affect the prediction accuracy, such as proper sub-grid scale (SGS) modelling, numerical dissipation and dispersion, boundary condition and so on. Proper grid length scale is one of the key parameters and it greatly influences the LES quality. For example, Léonard et al. (2014) compared the LES and RANS results for the sub-sonic turbine flow with relative coarse mesh which did not provide sufficient grid resolution to

resolve the small-scale turbulent structures. They found that the velocity profile in the boundary layer was well resolved by the RANS method; however, the LES method predicted poor results of the velocity profile in the boundary layer. Their study shows that the LES method is sensitive to the grid density and with insufficient mesh resolution LES performs worse than RANS.

The basic idea of the LES method is to resolve the large-scale turbulent structures and to model the small-scale part which is always isotropic and computational-demanding. The modelled term of these small-scale turbulent structures is represented by the SGS modelling. Implicit filtering operation is widely used in existing LES simulations and the filter width is the grid length. With smaller grid length, larger fraction of the turbulent structures are resolved by the mesh and thus the accuracy is improved. However, this raises bigger challenge in the computational cost, especially for turbulent flow with high Reynolds number. As a result, considering the limited computer resource and the requirement of fast-turnaround simulation, it is favourable to conduct LES with the mesh which achieves a balance between the accuracy and computational expense.

Many authors have devoted to propose LES quality index to assess the error of LES simulations. Geurts and Fröhlich (2002) suggest the sub-grid activity parameter

and sub-grid resolution parameter to assess the LES accuracy, which measures the relative turbulent dissipation rate and the ratio of the mesh spacing to the filter width. The sub-grid activity parameter is close to 1 for the LES simulations, which is not sensitive to the grid resolution (Celik, Cehreli, and Yavuz 2005), and the sub-grid resolution parameter is always 1 for the implicit filtering operation; so, these two parameters are not suitable to assess the LES errors with grid resolution. Directly considering the basic hypothesis of the LES method, the filter width should have the same order of magnitude as the inertial scale to ensure that the modelled turbulent structures are isotropic, so the error of the LES simulations can be assessed by comparing the grid spacing to some turbulent scales. For example, Celik, Cehreli, and Yavuz (2005) proposed a LES quality index based on the turbulence Reynolds number and the ratio of grid spacing to the Kolmogorov scale which should be estimated from the existing results. With further analyses, Celik, Cehreli, and Yavuz (2005) related this index to the ratio of efficient turbulent eddy viscosity to the molecular viscosity. From another point of view, Pope (2000) suggested that the modelled ratio of the total turbulent kinetic energy should be smaller than 0.2. The resolved turbulent kinetic energy can be directly identified from the LES results, but the modelled part should be estimated. Deardorff (1970) estimated the modelled turbulent kinetic energy from the turbulent eddy viscosity. Knopp et al. (2010) used the scale similarity assumption to estimate the SGS velocity, and then obtained the modelled turbulent kinetic energy.

For simple geometry, LES grid can be generated with some well-established guidelines. For example, to resolve more than 90% turbulent kinetic energy, Chapman (1979) suggested that $\Delta x^+ \approx 100$, $\Delta z^+ \approx 20$, $\Delta y^+ \approx 1 \sim 2$ near the wall for the wall-resolved LES simulation, and about 2500 points are necessary to resolve the turbulent eddies in the cubic computational volume of δ^3 exterior to the viscous sublayer ($y^+ \leq 100$), where δ is the boundary layer thickness. However, in practical LES simulations, the boundary layer thickness varies in different regions. What is more, the strong shear flow or large separation outside of the boundary layer adds more difficulties, as their positions and scales can be hardly accurately estimated before the simulation. To ensure the accuracy of LES, one possible way is to generate a super fine mesh; however, it is intractable due to the computational cost. Another way is to conduct simulation with the baseline mesh which may provide insufficient grid resolution in some region. Then, the LES quality index is applied to check the accuracy. After that the baseline mesh is locally refined or coarsened with manual operation to obtain the proper grid, which can ensure accurate LES simulation

and avoids overlarge computational costs. This method is feasible and the biggest shortcoming lies in the manual modification of the mesh because it consumes a large amount of labour work and is extremely difficult when dealing with complex geometry.

Adaptive mesh refinement (AMR) method can automatically refine the local mesh and is widely applied in many fields, see Berger and Oliger (1984), Nakahashi and Deiwert (1985), Pember et al. (1998), Tam et al. (2000), Bao, Chen, and Wu (2005), Sachdev, Groth, and Gottlieb (2005), Remaki and Habashi (2005), Gao and Groth (2006), Remaki and Habashi (2009), Su (2015) and Golay et al. (2015). Adopting the LES quality index as the refinement criterion, it is possible to automatically adjust the mesh according to the local resolution requirement and achieve improved accuracy and affordable cost simultaneously. This is rarely explored in the literature and it is the primary research interest in this paper. A refinement criterion suitable for LES is first proposed to estimate the proper grid length, then the AMR method is employed to automatically re-generate the mesh and a one-shot refinement strategy is used to further reduce the overall cost. Combining the LES quality index and AMR technology, an efficient LES solver balancing the accuracy and cost is developed. Current method is verified with the typical LES test case of flow over circular cylinder at $Re_D = 3900$. The results show that the developed LES refinement criterion and the one-shot refinement strategy work fairly well and the automatically refined mesh provides better agreement with the experiment.

This paper is organised as follows: the numerical solver is first described, and then the AMR-based LES method is introduced. The developed method is tested by the LES simulation of flow over circular cylinder at $Re_D = 3900$. Finally, the conclusion is given in the last section.

2. Numerical method

2.1. Unstructured finite volume solver

In the current work, a cell-centred unstructured code solving the filtered compressible Navier–Stokes equations is employed. This solver has been verified with the previous RANS and DDES simulations (Gou, Su, and Yuan 2016a, 2016b; Gou, Yuan, and Su 2017a, 2017b). For the LES simulation, current solver adopts the eddy viscosity hypothesis to obtain the turbulent stress tensor:

$$\tau^t - \frac{1}{3} \rho \tau_{kk}^t \mathbf{I} = 2\mu_{\text{sgs}} \left(\mathbf{S} - \frac{1}{3} (\nabla \cdot \mathbf{V}) \mathbf{I} \right) \quad (1)$$

where $\mathbf{V} = (\tilde{u}, \tilde{v}, \tilde{w})^T$ is the (Favre averaged) filtered velocity vector, \mathbf{S} is the strain rate tensor and \mathbf{I} is the

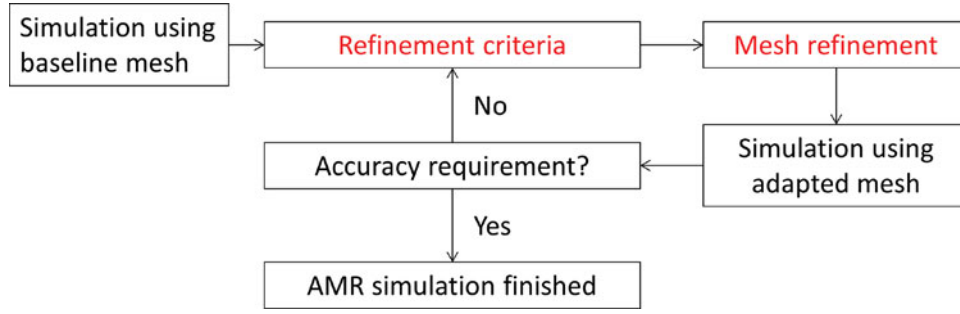


Figure 1. Flow chart of AMR method.

identity matrix. Several SGS models are implemented to calculate the turbulent eddy viscosity μ_{sgs} in the current solver, including the Smagorinsky model (Smagorinsky 1963), the wall-adapting local eddy (WALE) viscosity model (Nicoud and Ducros 1999), the σ model (Nicoud et al. 2011) and the volumetric strain-stretching model (Ryu and Iaccarino 2014). The WALE viscosity model is used in the following test case, without otherwise stated.

Ideal gas is adopted as the working fluid which satisfies $p = \rho RT$. For the treatment of the turbulent term in the energy equation, the heat flux \mathbf{q} is calculated as

$$\mathbf{q} = - \left(\frac{\mu_l c_p}{\text{Pr}_l} + \frac{\mu_{\text{sgs}} c_p}{\text{Pr}_t} \right) \nabla \tilde{T} \quad (2)$$

where μ_l is the molecular kinetic viscosity viscosity, \tilde{T} is the (Favre averaged) filtered static temperature, c_p is the ideal-gas heat capacity, Pr_l is the molecular Prandtl number and Pr_t is the turbulent Prandtl number.

The convective flux is discretised by a second-order MUSCL scheme based on an upwind flux difference splitting formulation. To improve the accuracy, the numerical dissipation is adaptively controlled by a blending function:

$$\mathbf{F}_n = \frac{1}{2} (\mathbf{F}(\mathbf{Q}_L) + \mathbf{F}(\mathbf{Q}_R)) - \frac{1}{2} \phi |A| (\mathbf{Q}_R - \mathbf{Q}_L) \quad (3)$$

where \mathbf{Q} is the filtered conservative variables, $\mathbf{F}(\mathbf{Q})$ is the convective flux, $\frac{1}{2} |A| (\mathbf{Q}_R - \mathbf{Q}_L)$ is the original numerical dissipation term of Roe scheme and ϕ is the blending function (Travin et al. 2002) calculated as

$$\phi = \phi_{\text{max}} \tanh(A^{CH1}) \quad (4)$$

where the variable A is calculated as

$$\begin{aligned} A &= CH2 \cdot \max\{C_s \Delta / L_{\text{turb}} / g - 0.5; 0\}, \\ L_{\text{turb}} &= \frac{(\mu_{\text{sgs}} + \mu_l)}{\rho (C_\mu^{3/2} K)^{1/2}} \\ K &= \max \left\{ \left[(\bar{S}^2 + \bar{\Omega}^2) / 2 \right]^{1/2}, 0.1 U_{\text{ref}} / L_{\text{ref}} \right\}, \\ g &= \tanh(B^4) \\ B &= CH3 \cdot \bar{\Omega} \cdot \max \left\{ \bar{\Omega}, \bar{S} \right\} / \\ &\quad \max \left\{ (\bar{S}^2 + \bar{\Omega}^2) / 2, 10^{-10} \cdot (U_{\text{ref}} / L_{\text{ref}})^2 \right\} \\ \bar{S} &= (2 \bar{S}_{ij} \bar{S}_{ij})^{0.5}, \bar{S}_{ij} = (\partial \tilde{u}_i / \partial x_j + \partial \tilde{u}_j / \partial x_i) / 2 \\ \bar{\Omega} &= (2 \bar{\Omega}_{ij} \bar{\Omega}_{ij})^{0.5}, \bar{\Omega}_{ij} = (\partial \tilde{u}_i / \partial x_j - \partial \tilde{u}_j / \partial x_i) / 2 \end{aligned} \quad (5)$$

where the above constants are $\phi_{\text{max}} = 1$, $CH1 = 3$, $CH2 = 1$, $CH3 = 2$.

A second-order centred scheme is used to discretise the viscous flux. The dual time-step method is employed for the unsteady simulation. The physical time term is discretised by the implicit second-order backward differentiation formula to allow large physical time step, and an implicit time integration scheme is adopted to treat the pseudo time term to allow large Courant–Friedrichs–Lewy (CFL) number.

2.2. Mesh refinement method

A high-order element-based unstructured AMR method (Gou, Yuan, and Su 2017a, 2017b) is employed in this work to refine the local mesh. Figure 1 shows the flow chart of the current AMR method.

Based on the simulation using the baseline mesh or the previous level adapted mesh, the proper refinement criteria are used to point out where the grid resolution is insufficient to resolve enough small-scale turbulent motions. These regions are then automatically and locally refined to generate the adapted mesh. The adapted mesh is then

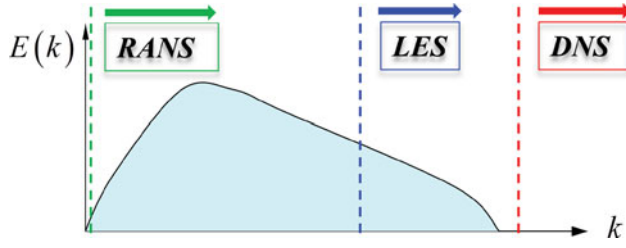


Figure 2. Sketch of energy spectrum for RANS, LES and DNS.

used to start a new simulation and this obtains more accurate results. This process may be repeated for several circles to obtain the expected accuracy.

Accurately representing the curved geometry during the mesh refinement is crucial to ensure the accuracy of the AMR solver. High-order element is introduced in our AMR method to construct the high-order formula between the computational space and parametric space, and linear adaptation is implemented in the parametric space which ensures good accuracy and robustness. This AMR strategy is verified by several two-dimensional/three-dimensional cases with complex geometry to improve the key feature prediction accuracy. Readers can refer to Gou, Yuan, and Su (2017b) for the detailed algorithms.

2.3. LES refinement criterion

Besides of the accurate and robust mesh refinement algorithm in the AMR process, LES refinement criterion is another key factor determining the accuracy and efficiency of the AMR-based LES method. As shown in Figure 2, the RANS method models all the turbulent energy and resolves the integral-scale structures with relatively coarse mesh.

The DNS method uses small grid length reaching the Kolmogorov scale and resolves all the turbulent structures with huge grid size. For the LES method, the large-scale turbulent eddies are resolved and the modelled small-scale turbulent motions are isotropic. Inspired by the basic hypothesis of the LES method and the proposed LES quality index to assess the LES simulation errors in the literature, there exist two ways to construct the LES refinement criterion. One way is to guarantee that the modelled turbulent structures are isotropic according to the LES model. The turbulence scale needs to be estimated. The Taylor scale or Kolmogorov scale is compared with the filter width which is also the grid length for the widely used implicit filtering operation. The adaptive filter width will be located in the inertial range with this LES refinement criterion. Another way is to make sure that most of the turbulent kinetic energy is resolved. In the present work, the latter one is implemented.

For a reliable LES simulation, more than 80% turbulent kinetic energy should be resolved, as suggested by Pope (2000). Thus, the LES refinement criterion of element i can be constructed in the following form:

$$\phi_i^L = \frac{E_{\text{sgs}}}{E_{\text{sgs}} + E_R} \quad (6)$$

where $E_R = 1/2 \langle \tilde{u}_i' \tilde{u}_i' \rangle$ is the resolved turbulent kinetic energy by the previous LES simulation, and E_{sgs} is the modelled turbulent kinetic energy. The latter one cannot be directly obtained from the previous LES results and should be further estimated. Different methods have been proposed to estimate the modelled turbulent kinetic energy. The modelled turbulent kinetic energy can be estimated from the turbulent eddy viscosity μ_{sgs} which directly represents the modelled small-scale structures in Equations (1) and (2) (Deardorff 1970):

$$E_{\text{sgs}} = (\nu_{\text{sgs}}/c\Delta)^2 \quad (7)$$

where $\nu_{\text{sgs}} = \mu_{\text{sgs}}/\rho$, Δ is the grid length scale and Deardorff (1970) recommended the constant $c \approx 0.094$. The choice of the constant c will be discussed later. This estimation has also been implemented by Benard et al. (2016) in their AMR-based LES simulation. Another way to estimate the modelled turbulent energy is to use the SGS velocity. Using the scale similarity assumption, the SGS velocity \mathbf{u}_{sgs} can be calculated as follows (Knopp et al. 2010):

$$\mathbf{u}_{\text{sgs}} = \tilde{\mathbf{u}} - \bar{\bar{\mathbf{u}}} \quad (8)$$

where $\tilde{\mathbf{u}}$ is the resolved instantaneous velocity vector in the LES simulation which is the filtered results of the actual instantaneous velocity vector, and the $\bar{\bar{\mathbf{u}}}$ represents another filtered results of the resolved instantaneous velocity vector calculated by the conventional integral:

$$\bar{\bar{\mathbf{u}}} = \int g_{\Delta}(\mathbf{x} - \mathbf{y}) \tilde{\mathbf{u}}(\mathbf{y}, \mathbf{t}) d\mathbf{y} \quad (9)$$

where g_{Δ} is the top hat filter function. In the calculation, this conventional integral of element i can be explicitly calculated using the direct neighbourhood:

$$\bar{\bar{\mathbf{u}}}^i = \frac{1}{N_i} \sum_j \tilde{\mathbf{u}}^j \quad (10)$$

where element j is the neighbour of element i , the summation is along the neighbourhood of element i and N_i is the number of this neighbourhood. With this SGS \mathbf{u}_{sgs} , the modelled turbulent kinetic energy can be calculated

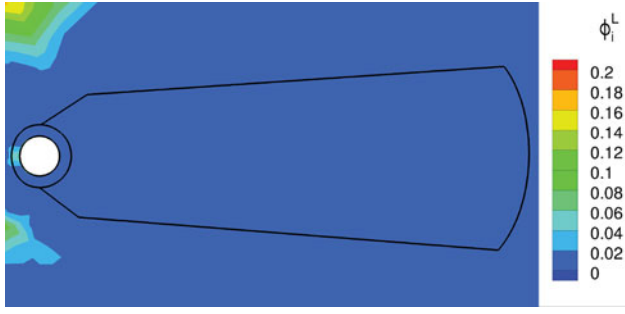


Figure 3. Modelled ratio of the turbulent kinetic energy of the baseline mesh with the estimation of Equation (11), flow over circular cylinder at $Re_D = 3900$.

as follows:

$$E_{sgs} = \frac{1}{2} \langle \mathbf{u}_{sgs}^2 \rangle \quad (11)$$

where $\langle \cdot \rangle$ denotes the time-average. This estimation has been implemented by Reuß (2016) in their AMR-based hybrid RANS/LES simulation. However, this method uses the local spatial integral to obtain the SGS velocity, and may miss the large-scale unsteady flow structure. It works for statistically steady flow, otherwise it may underestimate the modelled turbulent kinetic energy, especially for the flow with large-scale periodic flow motion as shown in Figure 3 in the following part. Besides, when the grid resolution is small enough satisfying the DNS requirement, the turbulent eddy viscosity will almost vanish, and the LES simulation becomes a DNS simulation. However, this conventional integral will also result in non-zero SGS velocity and lead to over-estimation of the turbulent kinetic energy. Considering the above two shortcomings of this estimation, the first estimation using Equation (7) is implemented to construct the LES refinement criterion in the present work.

With the modelled turbulent kinetic energy, the LES refinement criterion calculated by Equation (6) is obtained. When the LES refinement criterion satisfies $\phi_i^L \leq 0.2$, the resolved turbulent kinetic energy is larger than 80% and the local grid resolution is sufficient for the accurate LES simulation. Otherwise, the local mesh needs to be refined. Because the turbulent eddy viscosity in the LES method theoretically varies as the filter width with a 4/3 power law (Pope 2000):

$$\nu_{sgs} \sim \Delta^{4/3} \quad (12)$$

Combining Equations (6), (7), (12) and the assumption that the total turbulent kinetic energy ($E_{sgs} + E_R$) is almost constant along adaptation, the proper grid length Δ_{AMR} which satisfies the LES accuracy requirement $\phi_i^L =$

0.2 can be calculated as follows:

$$\Delta_{AMR} = \Delta \cdot \left(\frac{0.2}{\phi_i^L} \right)^{3/2} \quad (13)$$

where Δ is the grid length of the previous simulation mesh. In actual application, if the mesh is not allowed to be coarsened, the estimated grid length Δ_{AMR} is modified as follows:

$$\Delta_{AMR} = \Delta \cdot \max \left\{ \left(\frac{0.2}{\phi_i^L} \right)^{3/2}, 1.0 \right\} \quad (14)$$

Further considering the turbulence structures in real applications, not all the space has strong turbulent motions. In region with weak turbulence, both E_{sgs} and E_R are of small amplitude and the calculated LES refinement criterion using Equation (6) may contribute to large error due to spurious noise. In this case, the unwanted over-refinement will take place. To alleviate this problem, Equation (14) is modified and the final estimated grid length Δ_{AMR} can be calculated as follows:

$$\Delta_{AMR} = \begin{cases} \Delta \cdot \max \left\{ \left(\frac{0.2}{\phi_i^L} \right)^{3/2}, 1.0 \right\} & E_{sgs} + E_R > 0.1E_k \\ \Delta & E_{sgs} + E_R \leq 0.1E_k \end{cases} \quad (15)$$

where E_k is the local kinetic energy of the averaged flow field and it means that the AMR process is considered only in the region containing rich turbulent fluctuations.

In practical application, the baseline mesh is used to perform the first LES simulation, and then LES refinement criterion can be calculated from this result. If some physical features are also concerned, such as the shock wave or strong vortex, additional refinement criteria can be also applied here. In the refinement process two different choices, cycled refinement and one-shot refinement, can be selected, as shown in Figure 4.

Also note that in our AMR solver the resolution ratio between two neighbouring elements is not allowed to exceed two, in order to avoid too large element size change.

- (1) Cycled refinement: it is the same as the common AMR strategy where a series of LES simulations are conducted and current mesh in use is based on the former simulation. As sketched in Figure 4(a), this method continuously refines the mesh and leads to several LES simulations.
- (2) One-shot refinement: in this method only two LES simulations are conducted. With the LES results from the baseline mesh, the proper grid length

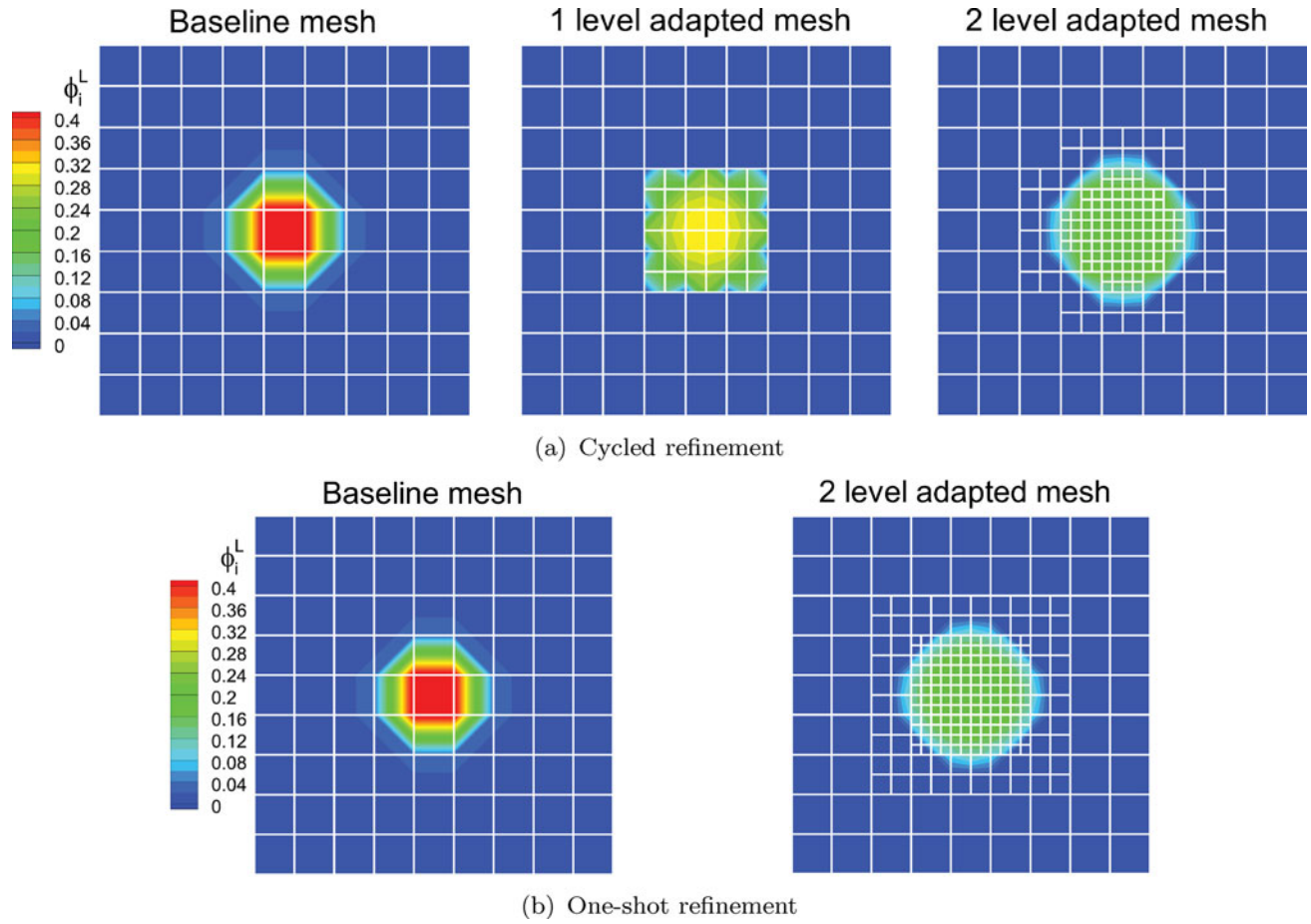


Figure 4. Sketch of cyclic and one-shot refinement methods.

scale is estimated using Equation (15) and then this information is fed into the mesh manipulation procedure. Then, the baseline mesh is refined several times, until the local mesh size Δ is smaller than the estimated Δ_{AMR} . This process is sketched in Figure 4(b).

Comparing the above two strategies, the one-shot refinement contains only two LES simulations and it consumes less computational cost; however, it may encounter some accuracy issues because the refinement criterion is computed using the baseline mesh. This method assumes that with the refined mesh $\phi_i^L \leq 0.2$ is assured and Δ_{AMR} given by Equation (15) is an *a-priori* estimation. If the baseline mesh is not too coarse, this method is reasonable. The cycled refinement strategy is more accurate, as $\phi_i^L \leq 0.2$ with the final mesh is guaranteed; however, more than two LES simulations are required and this results in exceedingly computational expense. For the balance between the accuracy and efficiency, these two choices can be selected for different cases.

Also it has to be noted that current method also applies in the hybrid RANS/LES simulations where LES mode is activated in the off-wall region. In this case Equation (15) should be applied only in the LES region and in the RANS region, some existing methods (Su 2015; Gou, Yuan, and Su 2017b) are available.

3. Numerical example

3.1. Description of the test case

The flow over circular cylinder at $Re_D = 3900$ is simulated with the LES method. This test case is a typical LES validation example, which is simulated by several authors with the LES or DNS method (Breuer 1998; Fröhlich et al. 1998; Ma, Karamanos, and Karniadakis 2000; Kravchenko and Moin 2000; Franke and Frank 2002; Dong et al. 2006; Parnaudeau et al. 2008; Meyer, Hickel, and Adams 2010; Lysenko, Ertesvåg, and Rian 2012). Also, several groups of experimental results are available (Norberg 1987; Lourenco and Shih 1993; Ong and Wallace 1996; Parnaudeau et al. 2008). For typical

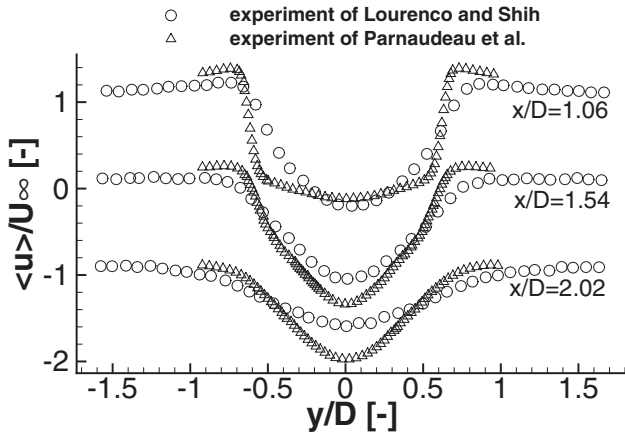


Figure 5. Mean streamwise velocity distribution of experimental results in the very near wake zone.

flow over circular cylinder, when the Reynolds number is smaller than 100, the whole flow field is laminar and the periodic Karman vortex street continues downstream of the cylinder. With the increase of the Reynolds number, the instabilities arise in the downstream separation zone. At $Re_D = 3900$, transition takes place in the separation zone, and the cylinder wake consists of turbulent flows.

To make it more clear, the wake region is divided into three zones: the very near wake zone ranging from the cylinder to 3 diameters, the wake core zone ranging from 3 diameters to 10 diameters and the far wake zone downstream of 10 diameters. It should be noted that different experimental results can be found for the very near wake zone in the literature.

Figure 5 shows the experimental mean streamwise velocity distributions which are normalised by the free-stream velocity U_∞ by different authors in the very near wake zone. Obviously different mean streamwise velocity distributions appear in the very near wake zone, especially at $x/D = 1.06$. Lourenco and Shih obtained the V-type velocity distribution at $x/D = 1.06$, but Parnaudeau et al. obtained the U-type velocity distribution here. The different velocity distributions in the very near wake zone also influence the separation length. The experimental separation length of Parnaudeau et al. is larger than the experimental results of Lourenco and Shih, which is shown later in Figure 6. Different LES or DNS simulations replicated these two types of streamwise velocity distribution at $x/D = 1.06$. Some results predicted the U-type velocity distribution (Beaudan and Moin 1994; Ma, Karamanos, and Karniadakis 2000; Kravchenko and Moin 2000; Franke and Frank 2002; Dong et al. 2006; Parnaudeau et al. 2008; Meyer, Hickel, and Adams 2010; Lysenko, Ertesvåg, and Rian 2012), while other results

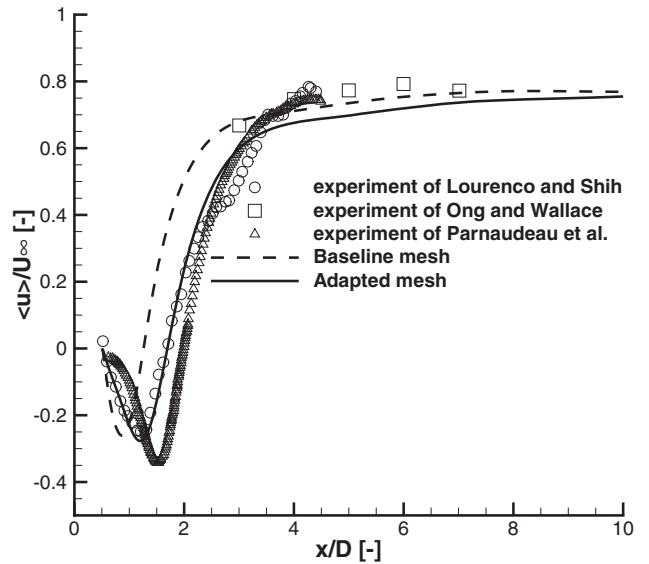


Figure 6. Mean streamwise velocity distribution on the center-line downstream of the cylinder, flow over circular cylinder at $Re_D = 3900$.

predicted the V-type velocity distribution (Ma, Karamanos, and Karniadakis 2000; Fröhlich et al. 1998; Dong et al. 2006; Lysenko, Ertesvåg, and Rian 2012). Further downstream, these differences begin to vanish in the wake core zone and far wake zone.

Ma, Karamanos, and Karniadakis (2000) systematically investigated the behaviour of the very near wake flow prediction by DNS and LES simulations. They proposed that this region is dominated by the shear-layer dynamics and is very sensitive to the disturbances. Many factors including the cylinder aspect ratio, downstream disturbance, cylinder diameter, channel blockage and so on, will influence the disturbance evolution of the shear flow in the separation zone, and may result in different velocity distribution types and separation lengths in the very near wake zone. Ma et al. simulated cases with different aspect ratios, and they predicted both the U-type and V-type velocity distributions at $x/D = 1.06$ with various aspect ratios. Besides of the influence of physical factors, the numerical methods may also influence the velocity distribution type near the cylinder. With the same aspect ratio, many authors predict different types with various numerical solvers. For example, with aspect ratio equals to 4, Meyer, Hickel, and Adams (2010) predict both the U-type and V-type velocity distributions at $x/D = 1.06$ with different grid topologies using the implicit LES simulation. Even with the same computational grid and numerical solver, different LES models (Smagorinsky model and dynamic k -equation SGS model, respectively) may also contribute to different velocity distribution types at $x/D = 1.06$ (Lysenko, Ertesvåg, and Rian 2012).

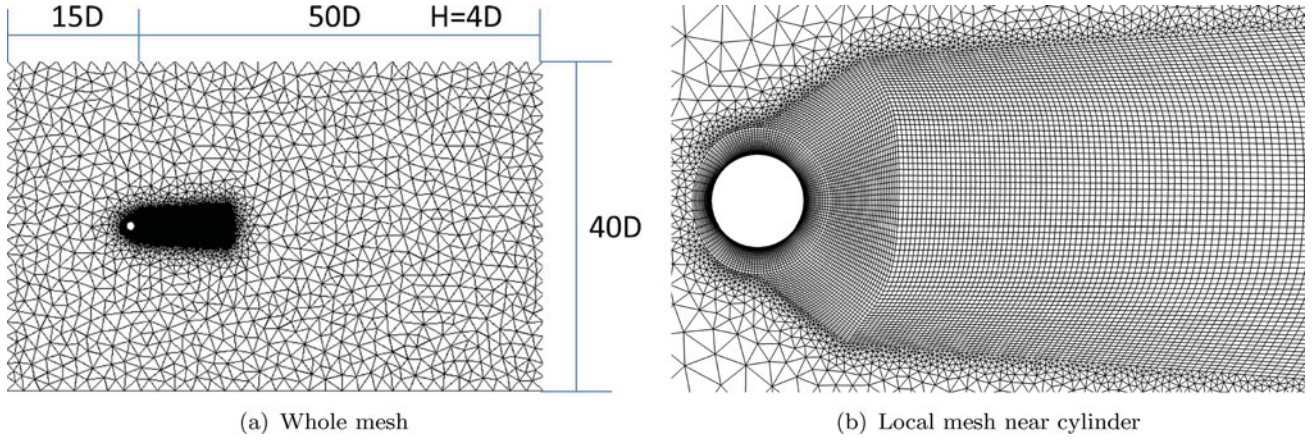


Figure 7. Baseline mesh of flow over circular cylinder at $Re_D = 3900$.

3.2. Simulation set-up

In order to perform the AMR-based LES simulation for the flow over circular cylinder, the baseline mesh is first generated, as shown in Figure 7.

The cylinder diameter is D . The computational domain is large enough to prevent the far-field boundary reflection, with $15D$ upstream of the cylinder, $50D$ downstream of the cylinder and $40D$ in the crosswise direction. The spanwise height is $4D$ which is a bit larger than the widely used spanwise height πD in the existing LES or DNS simulations. Near the cylinder region and in the wake region downstream of the cylinder, there exist transition and turbulent flows. These structures are the primarily concerned flows of this simulation, so hexahedral elements with relatively higher grid resolution are used in these regions. Other region is filled with prisms with relatively low resolution. The baseline mesh consists of 817k elements. Considering the boundary condition, non-slip boundary condition is set on the cylinder surface, and the far-field boundary condition is set in the outer space. The free-stream Mach number is $Ma_\infty = 0.15$, and the free-stream static temperature is $T_\infty = 280$ K. Periodic boundary condition is applied in the span-wise direction.

In the present LES simulation, WALE model is adopted to treat the turbulent terms. The dual time-step method is used for the time advancing. The physical time step is $0.006D/U_\infty$, and within every physical step the residual is reduced by at least three orders of magnitude. The baseline LES simulation is initialised from the RANS result. After time advancement for 40,000 physical time steps (about 48 vortex shedding periods), the initial transient is washed out and statistically steady-state is reached. Then, time-averaging is taken during the following 100 vortex shedding periods. The obtained mean flow field provides necessary information required by the AMR procedure and one-shot refinement is used in this example. Also, the

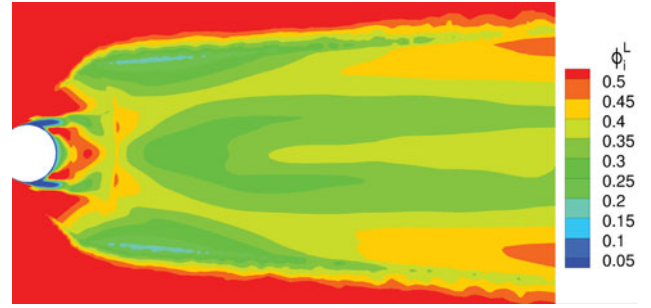


Figure 8. Modelled ratio of the turbulent kinetic energy of the baseline mesh, flow over circular cylinder at $Re_D = 3900$.

instantaneous results from the baseline mesh are used to initialise the LES computation using the refined mesh. This largely reduces the transient stage of the latter LES simulation.

Figure 8 shows the modelled ratio of the turbulent kinetic energy ϕ_i^L (calculated using Equation (6)) of the baseline mesh. As shown in Figure 8, the modelled turbulent kinetic energy ratio ϕ_i^L exceeds 0.2 in most regions of the very near wake and wake core zones. This indicates that the grid resolution is insufficient for the LES simulation, especially in the strong shear-layer near the cylinder where transition occurs. The baseline mesh leads to inaccurate prediction of the transition motion and instabilities in the very near wake zone, and subsequently causes large errors of the mean flow field prediction, as given in the next section. Outside the wake region, the turbulence is very weak; however, the modelled ratio ϕ_i^L is of large amplitude due to the inaccurate estimation of the turbulent kinetic energy. As shown in the next section, the grid resolution in this region is sufficient for LES simulation and does not need to be refined. This highlights the importance of the modification in the weak turbulence region, as given in Equation (15). Replacing Equation

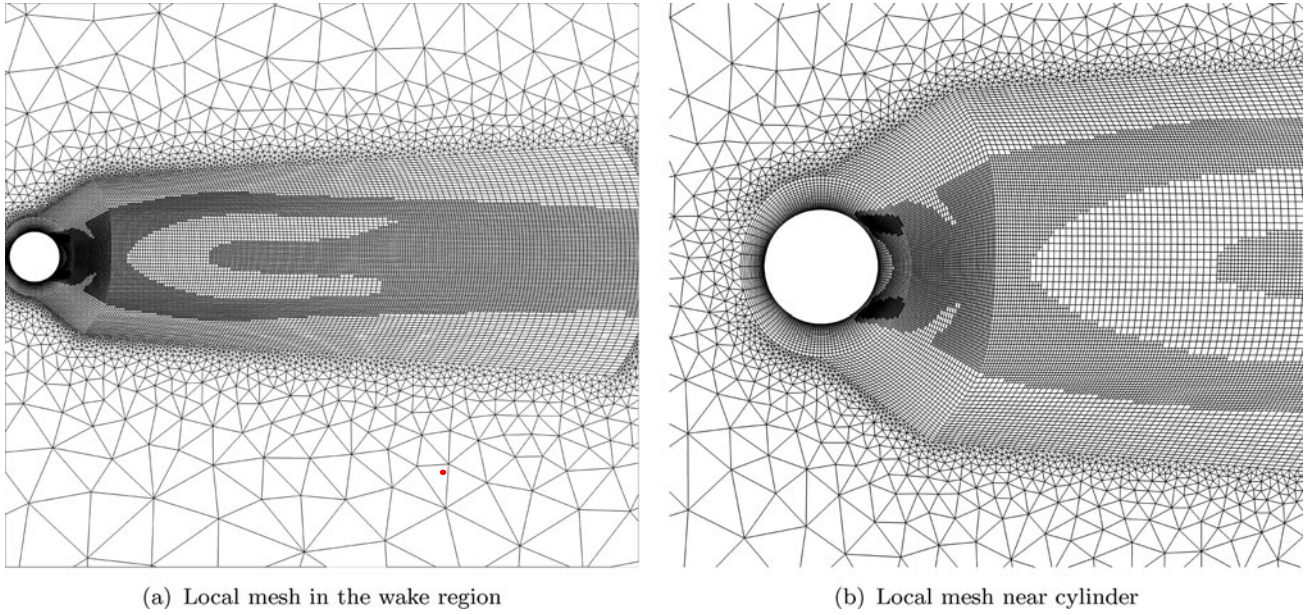


Figure 9. Adapted mesh with current one-shot refinement strategy.

(14) by Equation (15) can avoid the unnecessary over-refinement to reduce the mesh size and computational cost.

The above refinement criterion uses Equation (7) to estimate the modelled turbulent kinetic energy. Figure 3 shows the estimated modelled turbulent kinetic energy ratio with Equation (11). The black lines mark the region near the cylinder and the wake region which are filled with hexahedral elements in Figure 3, and the estimated modelled ratio is nearly zero in these regions which is obviously unreasonable. As shown in Figure 3, if Equation (11) is implemented for the flow with remarkable periodic motions, the modelled turbulent kinetic energy is greatly under-estimated, especially in the wake region with strong turbulence.

Hence, the second estimation should be carefully implemented for large-scale periodic flow and is not appropriate for the present case.

To improve the resolved turbulent kinetic energy ratio and accuracy of the LES simulation, the proper grid length Δ_{AMR} is estimated by Equation (15) based on the LES results of the baseline mesh. Based on the estimated grid length, current one-shot refinement is conducted and the baseline mesh is locally refined for two-times. Most of the refinement takes place in the very near wake and wake core regions. The adapted mesh contains 2.655 million elements, as shown in Figure 9. The constant c in Equation (7) greatly influences the predicted necessary grid length. The recommended value 0.094 by Deardorff (1970) is adopted in the present work. In region where the predicted $\Delta_{\text{AMR}}/\Delta = 4$, if constant c changes to be

0.083, the predicted $\Delta_{\text{AMR}}/\Delta$ will change to be 4.68; if constant c changes to be 0.103, the predicted $\Delta_{\text{AMR}}/\Delta$ will change to be 3.42. Above results show that the obtained adapted mesh is sensitive to the choice of the constant c , so this constant should be determined carefully by theoretical analysis.

Table 1 shows the grid size in the AMR process.

If global refinement is conducted, to obtain similar resolution as the AMR mesh, the grid number will reach 52.288 M and it is obvious that the AMR method greatly reduces the cost. The time elapsed during the mesh refinement is on the order of one minute; on the other hand, far more labour work is required if the mesh is manually adjusted for similar quality.

3.3. Numerical results

Figure 10 shows the modelled ratio of the turbulent kinetic energy ϕ_i^L of the adapted mesh. Several streamlines are also given to mark the separation region near the cylinder. Comparing to the results of the baseline mesh shown in Figure 8, the resolved turbulent kinetic energy ratio obviously increases. In most regions of the very near

Table 1. Grid size in the AMR process, flow over circular cylinder at $Re_D = 3900$.

| Mesh | Number of elements |
|-----------------------|--------------------|
| Baseline mesh | 0.817M |
| AMR refined mesh | 2.655M |
| Globally refined mesh | 52.288M |

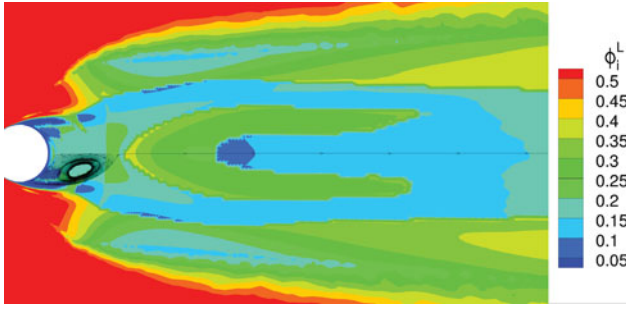


Figure 10. Modelled ratio of the turbulent kinetic energy of the adapted mesh, flow over circular cylinder at $Re_D = 3900$.

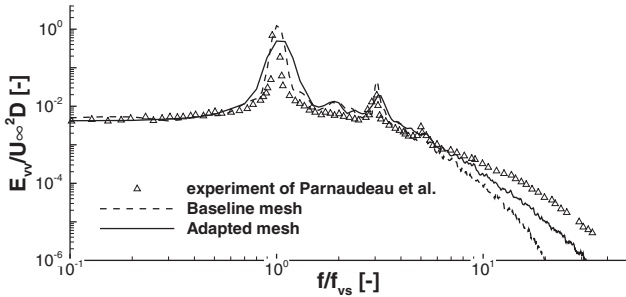


Figure 11. One-dimensional spectra of the transverse velocity at $x/D = 5$, flow over circular cylinder at $Re_D = 3900$.

wake and wake core zones, the modelled ratio of the turbulent kinetic energy is smaller than 0.2, indicating the grid resolution is sufficient for accurate LES simulation. The transition region in the strong shear-layer near the cylinder is well locally refined, and this is beneficial for the separation prediction in the very near wake zone. With current one-shot refinement strategy, the modelled ratio is around 0.3 in the other part of the very near wake and wake core zones. As explained in Section 2.3, the modelled turbulent kinetic energy ratio cannot be ensured to be below 0.2 in the whole region with strong turbulent structures. However, as shown in the following, the LES results of the adapted mesh are still in good agreement with the experimental results.

With more turbulent kinetic energy predicted by the adapted mesh, wider inertial range is obtained. Figure 11 shows the one-dimensional spectra of the transverse velocity at $x/D = 5$ in the wake region. The frequency is nondimensionalised by the wake shedding frequency f_{vs} , and the spectra using Welch method are span-wise averaged to increase the statistic sample. Comparing to the experimental results of Parnaudeau et al. (2008), the present LES simulations well predict the power spectral and the adapted mesh is obviously less dissipative than the baseline mesh.

To detailedly discuss the estimated necessary filter width, Figure 12 shows the ratio of the grid length

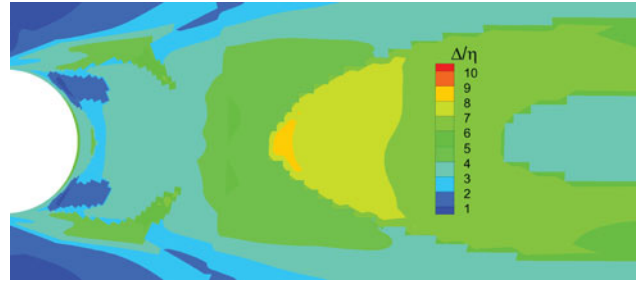


Figure 12. Scale ratio Δ/η of the adapted mesh, flow over circular cylinder at $Re_D = 3900$.

Δ (which is also the sub-grid filter scale) to the estimated Kolmogorov scale η of the adapted mesh. The Kolmogorov scale η is estimated as $\eta = (v^3/\varepsilon)^{0.25}$, where the dissipation rate is obtained as $\varepsilon = \langle \frac{\partial u'_i}{\partial x_k} \frac{\partial u'_i}{\partial x_k} \rangle$. It should be noted that the resolved fluctuating velocity u'_i using LES method will be smaller than the actual fluctuating velocity, so the estimated dissipation rate will be smaller than the physical one and this results in over-estimation of the Kolmogorov scale η . Even so, Figure 12 shows that the grid length scale of the adapted mesh is of the same order as the estimated Kolmogorov scale, and this indicates the obtained adapted mesh has enough grid resolution to resolve the small-scale turbulent eddies in the wake region.

Higher grid resolution contributes to more abundant turbulent vortex structures. Figure 13 shows the three-dimensional vortex structure in the wake region marked Q criterion, which is coloured by the Mach number.

Comparing to the results of the baseline mesh, the adapted mesh has higher grid resolution in the wake region and predicts more abundant three-dimensional coherent structures.

To further compare the obtained time-averaged flow field with the experimental results, Table 2 shows the mean flow parameters predicted by the baseline mesh and the adapted mesh. Some experimental and DNS results in the literature are also given. As explained earlier, different experimental results exist in the literature. For the current LES simulations, the predicted St is almost the same between the baseline mesh and the adapted mesh. It is different from the experimental results of Ong and Wallace (1996), close to the experimental results of Parnaudeau et al. (2008) and almost the same as the DNS results of Dong et al. (2006).

Comparing the minimal mean streamwise velocity U_{min}/U_∞ on the centre-line downstream of the cylinder, the baseline mesh and the adapted mesh predict the same value -0.26 , which is almost the same as the experimental results of Lourenco and Shih (1993) and Parnaudeau et al. (2008). However, the recirculation

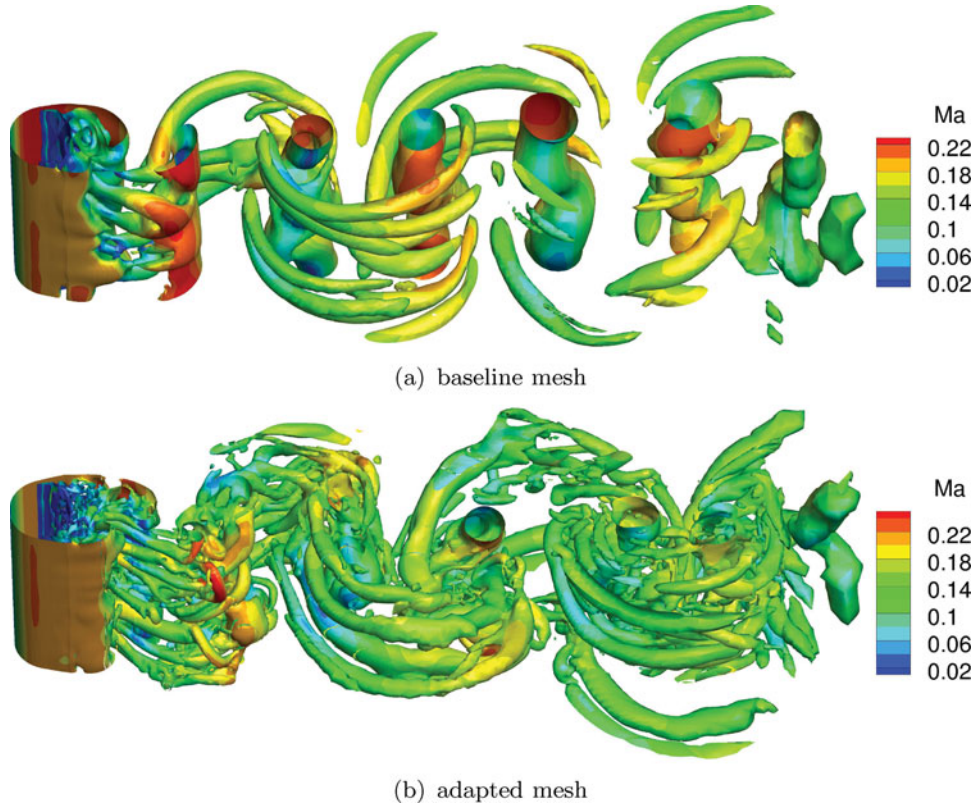


Figure 13. Isosurface of instantaneous Q criterion in the wake region, coloured by the Mach number.

length L_r/D is totally different between the baseline mesh and the adapted mesh. It is 0.757 in the baseline mesh results and much smaller than all the experimental results. The adapted mesh predicts circulation length 1.204, which is very close to the experimental results of Lourenco and Shih (1993) and different from the experimental results of Ong and Wallace (1996) and Parnaudeau et al. (2008).

Furthermore, the mean streamwise velocity distribution pattern at $x/D = 1.06$ is V-type for both the baseline mesh and adapted mesh, which is the same as the experimental results of Lourenco and Shih (1993). As explained above, different factors including the aspect

ratio, grid topology or LES model will influence the mean streamwise velocity distribution type at $x/D = 1.06$. Considering the fact that all the mean flow field is in good agreement with the experimental results shown later, this V-type velocity distribution is reasonable.

Figure 14 shows the time-averaged static pressure coefficient C_p distribution on the cylinder surface, where $C_p = \frac{p - p_\infty}{0.5 \rho_\infty U_\infty^2}$. Without experimental results at this Reynolds number, the experimental results of Norberg (1987) at $Re_D = 3000$ is given in Figure 14 as a reference, which is similar as the results at $Re_D = 3900$. The baseline mesh predicts lower mean static pressure coefficient. With mesh refinement, great improvement is obtained.

Table 2. Mean flow parameters, flow over circular cylinder at $Re_D = 3900$.

| | St | L_r/D | U_{min}/U_∞ | $(C_d)_{mean}$ | $(C_l)_{r.m.s}$ | $(C_d)_{r.m.s}$ |
|--------------------------------------|---------------|-------------|--------------------|----------------|-----------------|-----------------|
| Baseline mesh | 0.2021 | 0.757 | − 0.26 | 1.21 | 0.5193 | 0.0662 |
| Adapted mesh | 0.2023 | 1.204 | − 0.26 | 1.07 | 0.2311 | 0.0504 |
| Ong and Wallace (1996), exp | 0.215 | 1.4 | − 0.24 | - | - | - |
| Lourenco and Shih (1993), exp | - | 1.18 | − 0.25 | - | - | - |
| Parnaudeau et al. (2008), exp | 0.208 | 1.56 | − 0.26 | - | - | - |
| Dong et al. (2006), DNS | 0.203 | 1.36 | − 0.291 | - | - | - |
| Kravchenko and Moin (2000), LES | 0.21 | 1.35 | − 0.37 | 1.04 | - | - |
| Ouvrard et al. (2010), LES | 0.218 – 0.228 | 1.22 – 1.92 | - | 0.92 – 1.02 | 0.051 – 0.604 | 0.014 – 0.072 |
| Meyer, Hickel, and Adams (2010), LES | 0.215 | 1.18 | - | 1.07 | - | - |

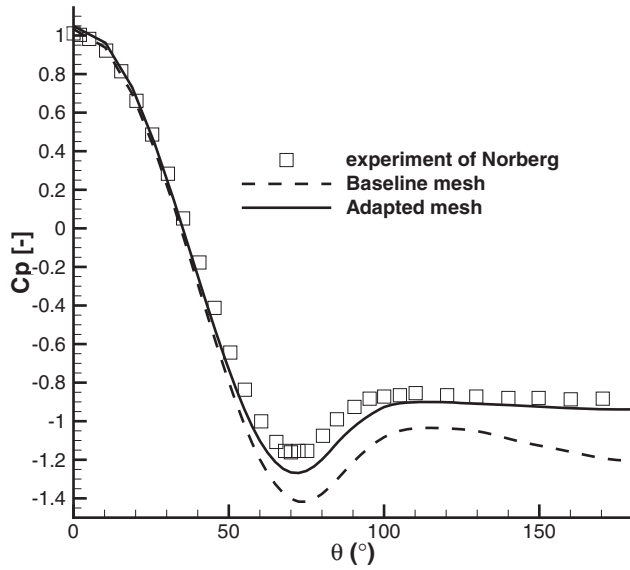


Figure 14. Mean static pressure coefficient C_p distribution on the cylinder surface, flow over circular cylinder at $Re_D = 3900$.

The results of the adapted mesh are in good agreement with the experimental results, in spite of still lower C_p for large θ which is also observed in the DNS results of Ma, Karamanos, and Karniadakis (2000).

Because of the lower mean static pressure coefficient in the rear of the wall, the predicted mean drag coefficient $\overline{C_p}$ is 1.21 by the baseline mesh and 1.07 by the adapted mesh, which is a bit larger than the experimental results of 0.99 ± 0.05 (from Kravchenko and Moin (2000)). Obviously the adapted mesh predicts better mean drag coefficient than the baseline mesh. The discrepancy of $(C_d)_{\text{mean}}$ predicted by the adapted mesh is small. Considering the fact that it is the same with the LES results of Fröhlich et al. (1998) and Meyer, Hickel, and Adams (2010) (the case using the curvilinear grid which also predicted the V-type streamline velocity distribution at $x/D = 1.06$), this discrepancy is acceptable and the adapted mesh well predicts the mean drag coefficient. The comparison of the root-mean-square values of both drag and lift coefficients are also given in Table 2 and it can be seen that they are slightly reduced with the refined mesh. Similar results have also been obtained by Ouvrard et al. (2010) who studied the effects of different SGS model and mesh resolution. They found that the higher the grid resolution, the lower the predicted root-mean-square values. Current AMR values are similar as their results using high grid resolution with the same WALE model (case F3 in Ouvrard et al. (2010)), and obviously better than the baseline mesh results.

Figure 6 shows the mean streamwise velocity distribution on the centre-line downstream of the cylinder of the baseline mesh and adapted mesh. The

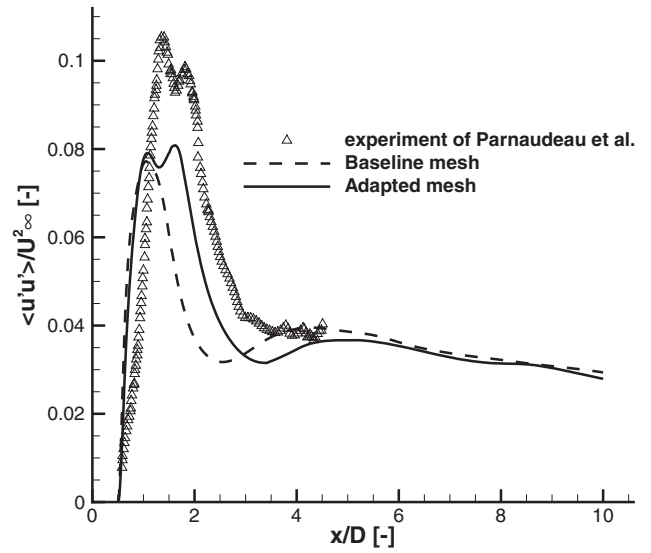


Figure 15. Streamwise velocity fluctuations on the centre-line downstream of the cylinder, flow over circular cylinder at $Re_D = 3900$.

experimental results of Lourenco and Shih (1993), Ong and Wallace (1996) and Parnaudeau et al. (2008) are also given. The predicted results of the baseline mesh clearly deviate from all the experimental results in the very near wake zone. The mesh refinement greatly improves the prediction accuracy. The results of the adapted mesh are in very good agreement with the experimental results of Lourenco and Shih (1993). This is consistent with the recirculation length given in Table 2. In the wake core zone, the predicted mean streamwise velocity is a bit lower than the experimental results, and this trend has also been observed in existing LES and DNS simulations.

Figure 15 shows the streamwise velocity fluctuations $\langle u'u' \rangle$ on the centre-line downstream of the cylinder. The experimental results of Parnaudeau et al. (2008) are given as a reference. Both sets of numerical results are a bit lower than the experiment. Considering that Parnaudeau et al. measure the U-type velocity distribution at $x/D = 1.06$, this discrepancy is acceptable. However, comparing these two numerical results, the adapted mesh predicts two peaks of $\langle u'u' \rangle$, while the baseline mesh predicts only one peak. The experimental results of Parnaudeau et al. (2008) show this double-peak distribution, and Norberg (1987) also measures this double-peak distribution for the flow over circular cylinder at $Re_D = 3000$ and $Re_D = 5000$. The adapted mesh correctly predicts this double-peak distribution and the baseline mesh fails due to insufficient grid resolution.

Figure 16 shows the mean streamwise velocity distribution in the very near wake zone $x/D \leq 3$. The velocity distribution at $x/D = 1.06$ of the baseline mesh and

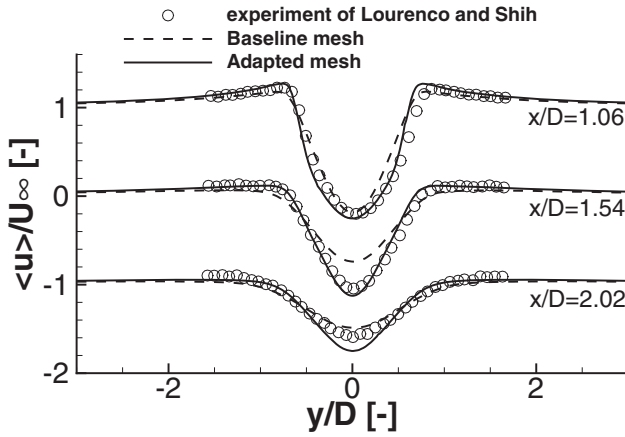


Figure 16. Mean streamwise velocity distribution in the very near wake zone, flow over circular cylinder at $Re_D = 3900$.

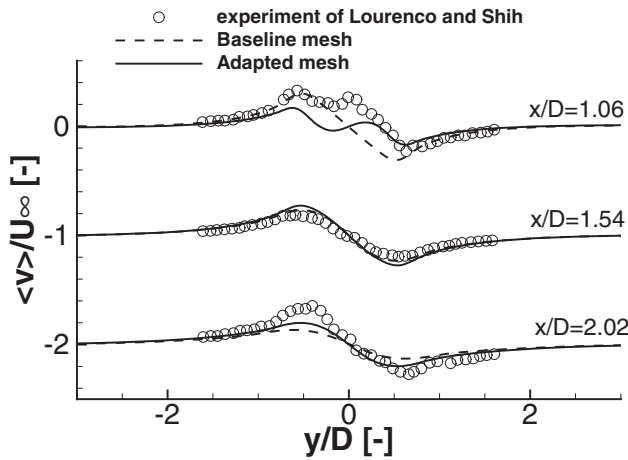


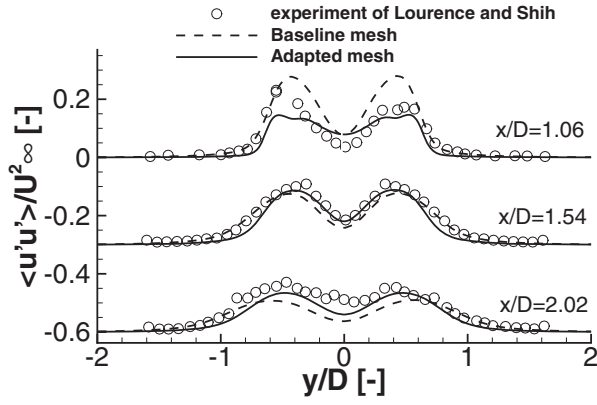
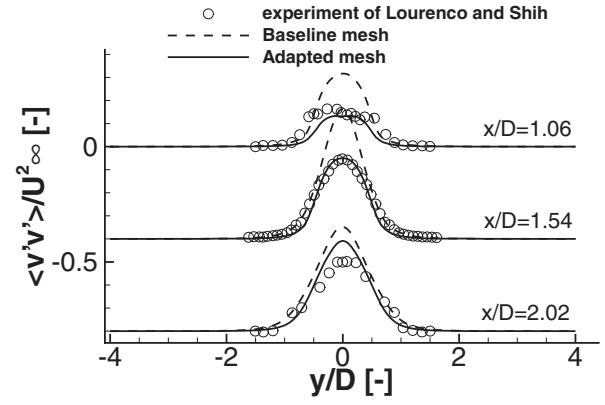
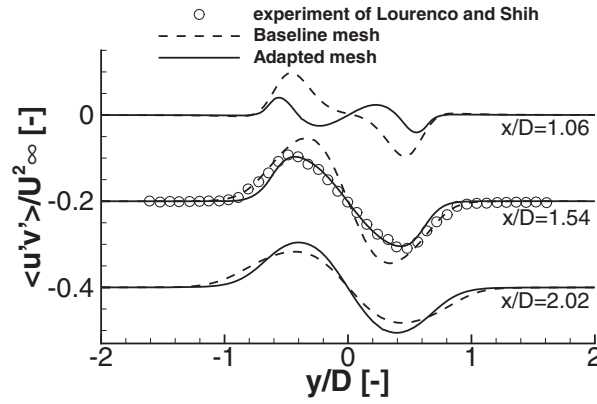
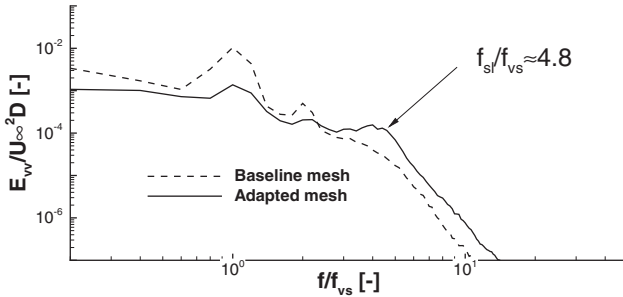
Figure 17. Mean transverse velocity distribution in the very near wake zone, flow over circular cylinder at $Re_D = 3900$.

adapted mesh is V-type as stated above. The results of the adapted mesh agree better with the experiment.

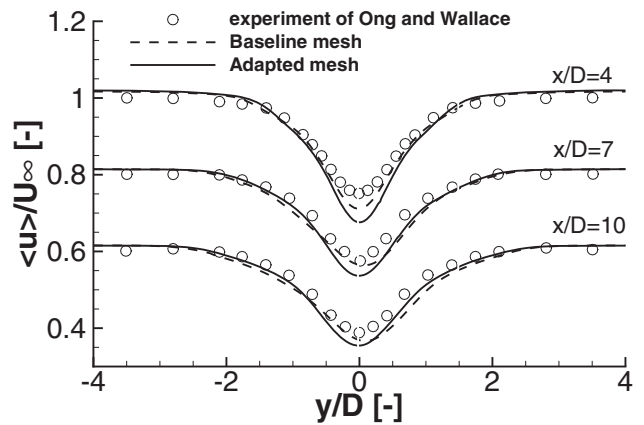
Figure 17 shows the transverse velocity distribution in the very near wake zone. It should be noted that the experimental results of Lourenco and Shih (1993) are carefully shifted to recover $\langle v \rangle = 0$ for large y/D , like other authors (Meyer, Hickel, and Adams 2010; Lysenko, Ertesvåg, and Rian 2012). This anomalous behaviour of the measured results may be due to the experimental disturbances. Despite this shift, the results of the adapted mesh are better than the baseline mesh, and correctly predict the double-peak distribution at $x/D = 1.06$. Although the predicted transverse velocity does not perfectly match the experimental results, comparing with existing LES or DNS simulations like Ma, Karamanos, and Karniadakis (2000), Meyer, Hickel, and Adams (2010) and Lysenko, Ertesvåg, and Rian (2012), our results of the adapted mesh are generally in good agreement with the experimental results.

Figure 18 gives the distributions of the streamwise and transverse velocity fluctuations, also the covariance of velocity fluctuation in the very near wake zone. As shown in Figure 18(a), Lourenco and Shih (1993) measured asymmetrical streamwise velocity fluctuation distribution at $x/D = 1.06$ because of experimental disturbances. The present LES results of the adapted mesh are in good agreement with the experimental results in the $y/D > 0$ part, but a bit lower in the $y/D < 0$ region. At downstream locations of $x/D = 1.54$ and $x/D = 2.02$, the predicted results of adapted mesh well match the experimental results. For the transverse velocity fluctuation, Figure 18(b) shows that the results of the adapted mesh are in good agreement with the experimental results. As shown in Figure 18(c), the adapted mesh accurately predicts the covariance of the velocity fluctuation at $x/D = 1.54$. Without the experimental results of Lourenco and Shih at $x/D = 1.06$ and $x/D = 2.02$, the quantitative errors between the LES results and the experimental results are not available, but the adapted mesh correctly predicts the double-peak distribution of velocity fluctuation covariance at $x/D = 1.06$ which is also predicted by Ma, Karamanos, and Karniadakis (2000). For all these velocity fluctuations in the very near wake zone, the results of the adapted mesh are in well agreement with the experimental results and obviously better than the baseline mesh. The local mesh refinement greatly improves the prediction accuracy.

In addition to the detailed analysis given in the above, the results from the baseline mesh and the AMR mesh are further compared using the one-dimensional spectra of the transverse velocity in the very near wake zone, as given in Figure 19. The unsteady information is collected at the mesh point $x/D = 0.5358$ and $y/D = 0.6415$ which locates in the shear-layer region, and the one-dimensional spectra there can reflect the Kelvin Helmholtz instability. Figure 19 demonstrates that with the baseline mesh only the wake vortex shedding frequency f_{vs} and its higher harmonics are captured. With the AMR mesh, broadband peaks f_{sl} corresponding to the frequencies of the shear-layer vortices are observed. These broadband peaks indicate that lots of vortices with a range of frequencies dominate the shear-layer region, and this phenomenon is according with the LES (Lysenko, Ertesvåg, and Rian 2012), DNS results (Dong et al. 2006) and the measurements (Prasad and Williamson 1997); however, with different numerical schemes Lysenko, Ertesvåg, and Rian (2012) predicted $f_{sl}/f_{vs} \approx 7 - 8$ with LES and Dong et al. (2006) predicted this value to be 7.83 using DNS. The generalised approximation from the experiment result of Prasad and Williamson (1997) indicated that $f_{sl}/f_{vs} = 5.99$ at $Re_D = 3900$. The prediction given by this work is a bit lower. As demonstrated by Lysenko, Ertesvåg, and

(a) streamwise velocity fluctuation $\langle u'u' \rangle$ (b) transverse velocity fluctuation $\langle v'v' \rangle$ (c) covariance of velocity fluctuation $\langle u'v' \rangle$ **Figure 18.** Velocity fluctuations in the very near wake zone, flow over circular cylinder at $Re_D = 3900$.**Figure 19.** One-dimensional spectra of the transverse velocity at the point $x/D = 0.5358$ and $y/D = 0.6415$, flow over circular cylinder at $Re_D = 3900$.

Rian (2012), numerical dissipation may lead to the underestimation of f_{sl} . From the comparison, current AMR helps to improve the prediction of Kelvin Helmholtz instability; however, current method should be further improved for an accurate prediction of f_{sl} in the shear-layer region.

**Figure 20.** Mean streamwise velocity distribution in the wake core zone, flow over circular cylinder at $Re_D = 3900$.

Figures 20 and 21 show the mean velocity distributions in the wake core zone $3 \leq x/D \leq 10$. In this region, only the experimental results from Ong and Wallace (1996) are available. Also note that Ong and Wallace measured

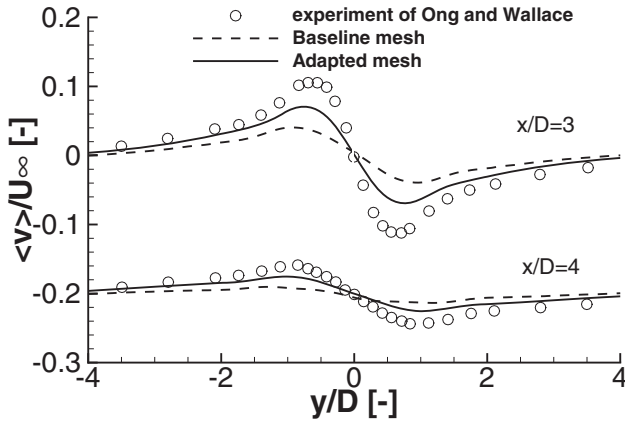


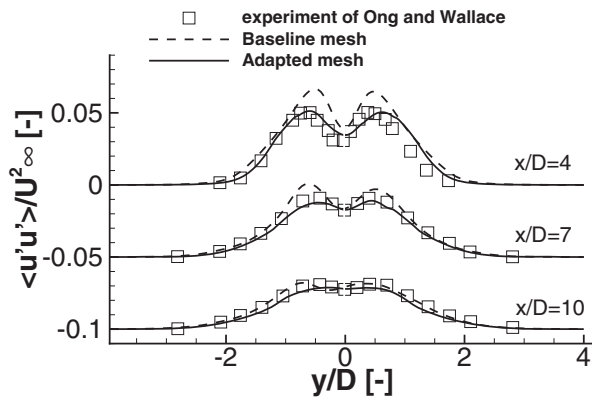
Figure 21. Mean transverse velocity distribution in the wake core zone, flow over circular cylinder at $Re_D = 3900$.

U-type of the mean streamwise velocity distribution at $x/D = 1.06$, which is different from the current LES simulation. However, the mean flow field in the wake core zone is mainly dominated by the vortex shedding motion and

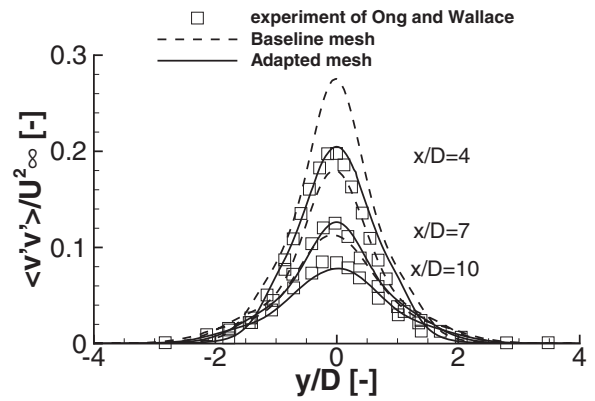
less influenced by the detailed separation structure in the very near wake zone; so, the experimental results of Ong and Wallace can provide a good reference for comparison. As given in Figure 21, the current LES results not perfectly but acceptably agree with the experimental results, and the adapted mesh is slightly better than the baseline mesh.

Figure 22 shows the distributions of the streamwise and transverse velocity fluctuations and the covariance of velocity fluctuation in the wake core zone. From the comparison it is clear that with the baseline mesh the turbulent fluctuations are mis-estimated due to the low mesh resolution and with the adapted mesh the results are much improved.

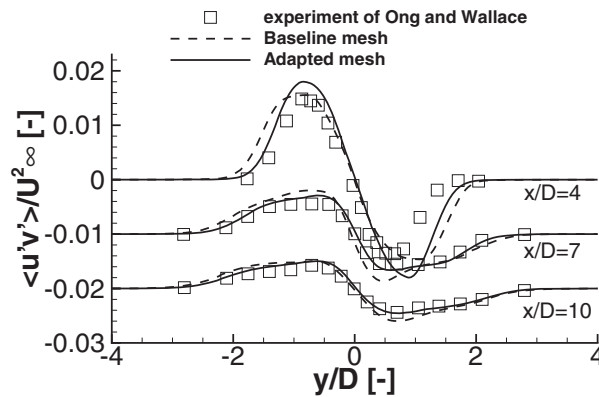
To summarise all the above, current LES refinement criterion reasonably estimates the proper grid length scale. With current one-shot refinement strategy, the refined mesh greatly improves the LES quality. The predicted mean flow field, also the turbulent fluctuations are in fairly good agreement with existing experimental results, especially in the very near wake region.



(a) streamwise velocity fluctuation $\langle u'u' \rangle$



(b) transverse velocity fluctuation $\langle v'v' \rangle$



(c) covariance of velocity fluctuation $\langle u'v' \rangle$

Figure 22. Velocity fluctuations in the wake core zone, flow over circular cylinder at $Re_D = 3900$.

4. Conclusions

An AMR-based LES method is developed in this work to automatically refine the mesh for the balance between accuracy and computational cost. Based on the basic hypothesis of LES, an LES refinement criterion representing the modelled kinetic energy ratio is developed. By considering its application in real-world flows, this criterion is further enhanced. Based on the LES results with the baseline mesh, the proper grid length scale for the accurate LES simulation is estimated. AMR method is employed to automatically refine the mesh. The one-shot refinement strategy is proposed which consumes only two LES simulations. The one-shot procedure and the common cycled refinement strategy are discussed.

The developed AMR-based LES method is verified with the circular cylinder case at $Re_D = 3900$ and the results are systematically compared with various experimental, LES and DNS results. Results show that the LES refinement criterion gives quite reasonable estimation of the proper grid length scale and marks the region requiring finer resolution. Compared to global refinement or manual refinement, AMR tool is quite efficient. The one-shot refinement strategy works well and the refined mesh yields more accurate results.

In the future work, current AMR-based LES solver will be further verified with more complex cases, also flows with higher Reynolds number.

Acknowledgments

Comments and suggestions from anonymous reviewers are deeply appreciated.

Disclosure statement

No potential conflict of interest was reported by the authors.

Funding

This work is supported by the National Natural Science Foundation of China [grant number 51506107], [grant number 51476082], [grant number 51136003].

References

- Bao, Gang, Zhiming Chen, and Haijun Wu. 2005. "Adaptive Finite-Element Method for Diffraction Gratings." *Journal of the Optical Society of America A* 22 (6): 1106–1114.
- Beaudan, Patrick, and Parviz Moin. 1994. *Numerical Experiments on the Flow Past a Circular Cylinder at Sub-Critical Reynolds Number*. Tech. rep. Stanford, CA: Stanford University.
- Benard, P., G. Balarac, V. Moureau, C. Dobrzynski, G. Lartigue, and Y. D'Angelo. 2016. "Mesh Adaptation for Large-Eddy Simulations in Complex Geometries." *International Journal for Numerical Methods in Fluids* 81 (12): 719–740.
- Berger, Marsha J., and Joseph Oliger. 1984. "Adaptive Mesh Refinement for Hyperbolic Partial Differential Equations." *Journal of Computational Physics* 53 (3): 484–512.
- Breuer, M. 1998. "Large Eddy Simulation of the Subcritical Flow Past a Circular Cylinder: Numerical and Modeling Aspects." *International Journal for Numerical Methods in Fluids* 28 (9): 1281–1302.
- Celik, I. B., Z. N. Cehreli, and I. Yavuz. 2005. "Index of Resolution Quality for Large Eddy Simulations." *Journal of Fluids Engineering* 127 (5): 949–958.
- Chapman, D. R. 1979. "Computational Aerodynamics Development and Outlook." *AIAA Journal* 17 (12): 1293–1313.
- Deardorff, J. W. 1970. "A numerical Study of Three-Dimensional Turbulent Channel Flow at Large Reynolds Numbers." *Journal of Fluid Mechanics* 41 (2): 453–480.
- Dong, S., Ge. Karniadakis, A. Ekmekci, and D. Rockwell. 2006. "A Combined Direct Numerical Simulation-particle Image Velocimetry Study of the Turbulent Near Wake." *Journal of Fluid Mechanics* 569 (12): 185–207.
- Duchaine, Florent, Nicolas Maheu, Vincent Moureau, Guillaume Balarac, and Stéphane Moreau. 2013. "Large-Eddy Simulation and Conjugate Heat Transfer Around a Low-Mach Turbine Blade." *Journal of Turbomachinery* 136 (5): 051015.
- Franke, J., and W. Frank. 2002. "Large Eddy Simulation of the Flow Past a Circular Cylinder at $Re_D=3900$." *Journal of Wind Engineering and Industrial Aerodynamics* 90 (10): 1191–1206.
- Fröhlich, J., W. Rodi, P. Kessler, S. Parpais, J. P. Bertoglio, and D. Laurence. 1998. "Large Eddy Simulation of Flow around Circular Cylinders on Structured and Unstructured Grids." *Notes on Numerical Fluid Mechanics* 66: 319–338.
- Gao, X., and C. P. T. Groth. 2006. "A parallel adaptive mesh refinement algorithm for predicting turbulent non-premixed combustions flows." *International Journal of Computational Fluid Dynamics* 20 (5): 349–357.
- Geurts, B. J., and J. Fröhlich. 2002. "A Framework for Predicting Accuracy Limitations in Large-eddy Simulation." *Physics of Fluids* 14 (6): L41–L44.
- Golay, Frederic, Mehmet Ersoy, L. Yushchenko, and Damien Sous. 2015. "Block-based Adaptive Mesh Refinement Scheme using Numerical Density of Entropy Production for Three-Dimensional Two-Fluid Flows." *International Journal of Computational Fluid Dynamics* 29 (1): 67–81.
- Gou, Jinlan, Xinrong Su, and Xin Yuan. 2016a. "Adaptive Mesh Refinement for DDES Simulation on Transonic Compressor Cascade with Unstructured Mesh." In *ASME, Paper No. GT2016-56925* edited by Tim Lieuwen, pp. V02CT39A034. Seoul, South Korea: ASME.
- Gou, Jinlan, Xinrong Su, and Xin Yuan. 2016b. "Investigation on the Adaptive Mesh Refinement Method with Unstructured Grid for Transonic Compressor." *Journal of Engineering Thermophysics* 37 (4): 729–733.
- Gou, Jinlan, Xin Yuan, and Xinrong Su. 2017a. "Adaptive Mesh Refinement Method-based Investigation of the Interaction Between Shock Wave, Boundary Layer, and Tip Vortex in a Transonic Compressor." *Proceedings of the Institution of Mechanical Engineers, Part G: Journal of Aerospace Engineering*. doi:10.1177/09554110016687142.
- Gou, Jinlan, Xin Yuan, and Xinrong Su. 2017b. "A High-Order Element-based Adaptive Mesh Refinement Strategy

- for Three-Dimensional Unstructured Grid.” *International Journal for Numerical Methods in Fluids* 85 (1): 538–560.
- Knopp, Tobias, Xiaoqin Zhang, Roland Kessler, and Gert Lube. 2010. “Enhancement of an Industrial Finite-Volume Code for Large-Eddy-Type Simulation of Incompressible High Reynolds Number Flow Using Near-Wall Modelling.” *Computer Methods in Applied Mechanics and Engineering* 199 (13): 890–902.
- Kravchenko, A. G., and P. Moin. 2000. “Numerical Studies of Flow Over a Circular Cylinder at $Re_D=3900$.” *Physics of Fluids* 12 (2): 403–417.
- Lardeau, Sylvain, Michael Leschziner, and Tamer Zaki. 2012. “Large Eddy Simulation of Transitional Separated Flow Over a Flat Plate and a Compressor Blade.” *Flow, Turbulence and Combustion* 88 (1–2): 19–44.
- Léonard, T., L. Y. M. Gicquel, and N. Gourdain. 2010. “Steady/unsteady Reynolds-Averaged Navier-Stokes and Large Eddy Simulations of a Turbine Blade at high Subsonic Outlet Mach number.” *Journal of Turbomachinery* 137 (4): 697–709.
- Léonard, Thomas, Laurent Y. M. Gicquel, Nicolas Gourdain, and Florent Duchaine. 2014. “Steady/Unsteady Reynolds-Averaged Navier-Stokes and Large Eddy Simulations of a Turbine Blade at High Subsonic Outlet Mach Number.” *Journal of Turbomachinery* 137 (4): 041001.
- Lin, Dun, Xinrong Su, and Xin Yuan. 2018. “DDES Analysis of wake Vortex Related Unsteadiness and Losses in the Environment of HPT Stage.” *Journal of Turbomachinery* 140: 041001.
- Lourenco, L. M., and C. Shih. 1993. “Characteristics of the Plane Turbulent Near Wake of a Circular Cylinder, a Particle Image Velocimetry Study.” Private communication cited in Ref. (Beaudan and Moin 1994).
- Lysenko, D. A., I. S. Ertesvåg, and K. Erik Rian. 2012. “Large-Eddy Simulation of the Flow Over a Circular Cylinder at Reynolds Number 3900 Using the OpenFOAM Toolbox.” *Flow, Turbulence and Combustion* 89 (4): 491–518.
- Ma, X., C. S. Karamanos, and G. E. Karniadakis. 2000. “Dynamics and Low-Dimensionality of a Turbulent Near Wake.” *Journal of Fluid Mechanics* 410: 29–65.
- McMullan, W. A., and G. J. Page. 2011. “Large Eddy Simulation of a Controlled Diffusion Compressor Cascade.” *Flow Turbulence and Combustion* 86 (2): 207–230.
- McMullan, W. A., and G. J. Page. 2012. “Towards Large Eddy Simulation of Gas Turbine Compressors.” *Progress in Aerospace Sciences* 52 (SI): 30–47.
- Memory, C. L., J. P. Chen, and J. P. Bons. 2016. “Implicit Large Eddy Simulation of a Stalled Low-Pressure Turbine Airfoil.” *Journal of Turbomachinery* 138 (7): 071008.
- Meyer, M., S. Hickel, and N. A. Adams. 2010. “Assessment of Implicit Large-Eddy Simulation with a Conservative Immersed Interface Method for Turbulent Cylinder flow.” *International Journal of Heat and Fluid Flow* 31 (3): 368–377.
- Michelassi, V., J. G. Wissink, and W. Rodi. 2003. “Direct Numerical Simulation, Large Eddy Simulation and Unsteady Reynolds-Averaged Navier-Stokes Simulations of Periodic Unsteady Flow in a Low-Pressure Turbine Cascade: A Comparison.” *Proceedings of the Institution of Mechanical Engineers Part A Journal of Power and Energy* 217 (4): 403–411.
- Nakahashi, Kazuhiro, and G. S. Deiwert. 1985. “A Practical Adaptive-Grid Method for Complex Fluid-Flow Problems.” In *Ninth International Conference on Numerical Methods in Fluid Dynamics*, edited by J. P. Boujot, 422–426. Berlin, Germany: Springer.
- Nicoud, F., and F. Ducros. 1999. “Subgrid-Scale Stress Modelling Based on the Square of the Velocity Gradient Tensor.” *Flow, Turbulence and Combustion* 62 (3): 183–200.
- Nicoud, Franck, Hubert Baya Toda, Olivier Cabrit, Sanjeeb Bose, and Jungil Lee. 2011. “Using Singular Values to Build a Subgrid-Scale Model for Large Eddy Simulations.” *Physics of Fluids* 23 (8): 085106.
- Norberg, Christoffer. 1987. “Effects of Reynolds Number and a Low-Intensity Freestream Turbulence on the Flow Around a Circular Cylinder.” *Chalmers University, Goteborg, Sweden, Technological Publications* 87 (2): 1–55.
- Ong, L., and J. Wallace. 1996. “The Velocity Field of the Turbulent Very Near Wake of a Circular Cylinder.” *Experiments in Fluids* 20 (6): 441–453.
- Ouvrard, Hilde, Bruno Koobus, Alain Dervieux, and Maria Vittoria Salvetti. 2010. “Classical and Variational Multiscale LES of the Flow Around a Circular Cylinder on Unstructured Grids.” *Computers and Fluids* 39 (7): 1083–1094.
- Papadogiannis, Dimitrios, Florent Duchaine, Laurent Gicquel, Gaofeng Wang, and Stéphane Moreau. 2016. “Effects of Subgrid Scale Modeling on the Deterministic and Stochastic Turbulent Energetic Distribution in Large-Eddy Simulations of a High-Pressure Turbine Stage.” *Journal of Turbomachinery*. doi:10.1115/1.4032844.
- Parnaudeau, Philippe, Johan Carlier, Dominique Heitz, and Eric Lamballais. 2008. “Experimental and Numerical Studies of the Flow Over a Circular Cylinder at Reynolds number 3900.” *Physics of Fluids* 20 (8): 085101. doi:10.1063/1.2957018.
- Pember, Richard B., Louis H. Howell, John B. Bell, Phillip Colella, William Y. Crutchfield, W. A. Fiveland, and J. P. Jessee. 1998. “An Adaptive Projection Method for Unsteady, Low-Mach number Combustion.” *Combustion Science and Technology* 140 (1–6): 123–168.
- Pope, S. B. 2000. *Turbulent Flows*. Cambridge, UK: Cambridge University Press.
- Prasad, Anil, and Charles H. K. Williamson. 1997. “The Instability of the Shear Layer Separating from a Bluff Body.” *Journal of Fluid Mechanics* 333: 375–402.
- Raverdy, B., I. Mary, P. Sagaut, and N. Liapis. 2003. “High-Resolution Large-Eddy Simulation of Flow Around Low-Pressure Turbine Blade.” *AIAA Journal* 41 (3): 390–397.
- Ray, P. K., and W. N. Dawes. 2009. “Detached-Eddy Simulation of Transonic Flow Past a Fan-Blade Section.” In *AIAA*, edited by D. Thompson, 2009–3221. Miami, FL: AIAA.
- Remaki, Lakhdar, and Wagdi Habashi. 2005. “Pacing CFD: Automatic Mesh Adaptation as an Efficient Tool to Improve CFD Accuracy.” *International Journal of Computational Fluid Dynamics* 19 (8): 571–580.
- Remaki, Lakhdar, and Wagdi G. Habashi. 2009. “Hermite-based Mesh Adaptation for Functional Outputs Improvement in Fluid Flow Simulation.” *AIAA Journal* 47 (8): 1965–1976.
- Reuß, Silvia. 2016. “A Grid-Adaptive Algebraic Hybrid RANS/LES Method.” PhD thesis. der Georg-August University School of Science.

- Riéra, William, Lionel Castillon, Julien Marty, and Francis Leboeuf. 2013. "Inlet Condition Effects on the Tip Clearance Flow with Zonal Detached Eddy Simulation." *Journal of Turbomachinery* 136 (4): 041018.
- Ryu, Sungmin, and Gianluca Iaccarino. 2014. "A Subgrid-Scale Eddy-Viscosity Model Based on the Volumetric Strain-Stretching." *Physics of Fluids* 26 (6): 065107.
- Sachdev, J. S., C. P. T. Groth, and J. J. Gottlieb. 2005. "A Parallel Solution-Adaptive Scheme for Multi-Phase Core Flows in Solid Propellant Rocket Motors." *International Journal of Computational Fluid Dynamics* 19 (2): 159–177.
- Sarkar, S., and P. R. Voke. 2006. "Large-Eddy Simulation of Unsteady Surface Pressure Over a Low-Pressure Turbine Blade Due to Interactions of Passing Wakes and Inflexional Boundary Layer." *Journal of Turbomachinery* 128 (2): 221–231.
- Smagorinsky, Joseph. 1963. "General Circulation Experiments with the Primitive Equations: I. The Basic Experiment." *Monthly Weather Review* 91 (3): 99–164.
- Su, Xinrong. 2015. "Accurate and Robust Adaptive Mesh Refinement for Aerodynamic Simulation with Multi-Block Structured Curvilinear Mesh." *International Journal for Numerical Methods in Fluids* 12 (77): 747–766.
- Taghavi-Zenouz, R., and S. Eslami. 2012. "Numerical Simulation of Unsteady Tip Clearance Flow in an Isolated Axial Compressor Rotor Blades Row." *Proceedings of The Institution of Mechanical Engineers Part C: Journal of Mechanical Engineering Science* 226 (C1): 82–93.
- Tam, A., D. Ait-Ali-Yahia, M. P. Robichaud, M. Moore, V. Kozel, and W. G. Habashi. 2000. "Anisotropic Mesh Adaptation for 3D Flows on Structured and Unstructured Grids." *Computer Methods in Applied Mechanics and Engineering* 189 (4): 1205–1230.
- Travin, A., M. Shur, M. M. Strelets, and P. R. Spalart. 2002. "Physical and Numerical Upgrades in the Detached-Eddy Simulation of Complex Turbulent Flows." In *Advances in LES of Complex Flows*, edited by R. Friedrich and W. Rodi, 239–254. Berlin, Germany: Springer.
- Wang, Hao, Dun Lin, Xinrong Su, and Xin Yuan. 2017. "Entropy Analysis of the Interaction Between the Corner Separation and Wakes in a Compressor Cascade." *Entropy* 19 (7): 324. doi:10.3390/e19070324.
- You, Donghyun, Meng Wang, Parviz Moin, and Rajat Mittal. 2006. "Effects of Tip-Gap Size on the Tip-Leakage Flow in a Turbomachinery Cascade." *Physics of Fluids* 18 (10): 105102.